J. Fluid Mech. (2023), *vol*. 964, A37, doi:10.1017/jfm.2023.393

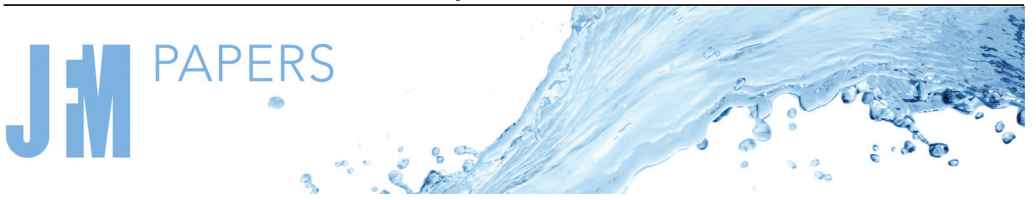

A decoupled mechanism of interface growth in single-mode hydrodynamic instabilities

Changwen Liu[1,2], **Hongzhi Wu-Wang**[2], **Yousheng Zhang**[1,3,†] **and Zuoli Xiao**[1,2,4,†]

[1]HEDPS, Center for Applied Physics and Technology, College of Engineering, Peking University, Beijing 100871, PR China

[2]State Key Laboratory for Turbulence and Complex Systems, College of Engineering, Peking University, Beijing 100871, PR China

[3]Institute of Applied Physics and Computational Mathematics, Beijing 100094, PR China

[4]Nanchang Innovation Institute, Peking University, Nanchang 330008, PR China

(Received 2 February 2023; revised 4 May 2023; accepted 5 May 2023)

One of the most significant issues in hydrodynamic interfacial instabilities is the growth rate of the interfacial perturbations, which plays an important role in both scientific research (e.g. supernova explosion) and engineering applications (e.g. inertial confinement fusion). Yet the underlying mechanisms of such flow phenomena remain unclear or controversial. In this paper the decoupled mechanisms of two effects are found to dominate the interface growth of the single-mode Rayleigh–Taylor instability (RTI) and Richtmyer–Meshkov instability (RMI) via Layzer's potential-flow model. One is the inertial effect induced by the interfacial density gradient and the acceleration, and the other is the frontal distortion effect stemming from interface shape evolution. The former determines the dominant features of interface evolution, while the latter influences the local concavity and convexity of growth rate such as the overshoot phenomenon. These two effects can be approximated as a linearly decoupled analytical solution if their nonlinear interaction term is neglected. With the decoupled solution, the theoretical growth rates agree well with high-fidelity numerical simulation results. The present result indicates that the long-time evolution of fluid interface in both RTI and RMI at all density ratios can be accurately predicted if both inertia and frontal distortion effects are taken into account. Furthermore, the strong dependence of instability evolution on initial amplitude is quantified based on the effects of decoupling, which sheds light on the physical origin of the overshoot phenomenon.

Key words: fingering instability, buoyancy-driven instability, nonlinear instability

† Email addresses for correspondence: zhang_yousheng@iapcm.ac.cn, z.xiao@pku.edu.cn

1. Introduction

Interfacial hydrodynamic instability occurs when an initially perturbed interface separating two fluids of different densities is subject to an acceleration (g) pointing from a heavy fluid to a light one or is impinged by a shock wave, which are known as the Rayleigh–Taylor instability (RTI) (Rayleigh 1883; Taylor 1950) and Richtmyer–Meshkov instability (RMI) (Richtmyer 1960; Meshkov 1969), respectively. During the development of these phenomena, light and heavy fluids penetrate into each other, giving rise to the formation of bubble-like (the portion of light fluid penetrating into heavy fluid) and spike-like (the portion of heavy fluid penetrating into light fluid) finger structures (Zhou 2017*a*,*b*). The growth rate of the finger structures can be of particular importance in nature and diverse engineering applications, such as the implosion of an inertial confinement fusion target (see, e.g. Betti & Hurricane 2016; Casey *et al.* 2017; Ding *et al.* 2017; Matsuo *et al.* 2021; Sabet *et al.* 2021), supersonic combustion in a scramjet (see, e.g. Yang, Kubota & Zukoski 1993; Niederhaus & Jacobs 2003) and the explosion of supernovae (see, e.g. Burrows 2000; Isobe *et al.* 2005).

Numerous theoretical, experimental and numerical studies have been conducted for the single-mode RTI and RMI since Taylor's seminal work in 1950 (Taylor 1950). Rayleigh (1883) studied the growth law of interface perturbation for the first time based on linear stability analysis, which was further developed by Taylor (1950). Subsequently, a number of milestone-like investigations extended the linear stability theory into the nonlinear regime (see, e.g. Lewis & Taylor 1950; Meshkov 1969; Jacobs & Catton 1988; Ristorcelli & Clark 2004; Ramaprabhu, Dimonte & ANDREWS 2005; Luo, Wang & Si 2013; Liu *et al.* 2018; Luo *et al.* 2018; Liang *et al.* 2019; Li *et al.* 2021; Yan *et al.* 2022; Lherm *et al.* 2022). Specifically, Lewis & Taylor (1950) reported the first experimental study on RTI, and Meshkov (1969) conducted the earliest RMI experiment using thin nitrocellulose membranes, which have sparked continuous interests in the experimental studies of both RTI and RMI (see, e.g. Allred, Blount & Miller 1953; Jacobs & Sheeley 1996; Waddell, Niederhaus & Jacobs 2001; Wilkinson & Jacobs 2007; Renoult, Rosenblatt & Carles 2015). In the community of numerical simulation, Daly (1967) was among the first to carry out two-dimensional (2-D) simulations of RTI flow. It was Tryggvason & Unverdi (1990) who conducted early three-dimensional (3-D) RTI flow. However, the computational challenges in the 3-D simulation of RTI flow led to the limitation of available numerical data. For general reviews of research advances on RTI and RMI, readers are referred to the articles by Sharp (1984), Brouillette (2002), Zhou (2017*a*,*b*), Zhou *et al.* (2019) and Zhou *et al.* (2021). One of the main issues in these studies is to predict the growth rate of interfacial perturbation or scaling of the mixed width, which can be used as a surrogate to characterize the degree of fluids mixing, and has been widely evaluated in previous studies. It needs to be mentioned, however, the mixed mass should be a more direct indicator on the evolution of interfacial mixing due to hydrodynamic instabilities (see, e.g. Zhou, Cabot & Thornber 2016). This is because the mixed mass is monotonically increasing with time and more important for realistic applications, such as inertial confinement fusion. Previous results confirmed that the interface evolution of single-mode RTI usually underwent a linear stage, nonlinear stage, quasi-steady stages with constant growth rate, and other possible stages (see figure 1 (Wei & Livescu 2012; Zhang & Guo 2016)). In this process, the growth rate in the nonlinear stage increases nonlinearly due to the gravity and shape variation of the interface, while in the quasi-steady stage, the growth rate tends to be constant due to the balance between buoyancy and drag forces on both sides of the interface, resulting in the self-similar evolution of the finger structure. Both stages are extremely important and have received extensive attention in previous investigations.

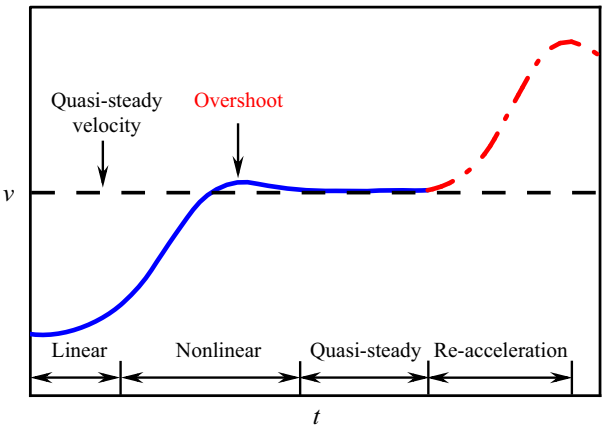

Figure 1. Schematic of different development stages of RTI based on the numerical result from Wei & Livescu (2012) and sketch map from Zhang & Guo (2016).

The advantages of theoretical study lay in its ability to provide a profound understanding for the flow phenomena observed in experiments and numerical simulations. Several influential theories have been established since Taylor's pioneering work, including the potential-flow model (Layzer 1955), Padé approximation approach (Zhang & Sohn 1997), vortex and vortex sheet models (Jacobs & Sheeley 1996; Matsuoka, Nishihara & Fukuda 2003), etc. Initially proposed to study the motion of vacuum bubbles with small initial perturbations, Layzer's potential-flow model (LPM) had been extensively adopted in studying fingering instabilities (see, e.g. Layzer 1955; Hecht, Alon & Shvarts 1994; Alon *et al.* 1995; Zhang & Sohn 1996; Mikaelian 1998; Zhang 1998; Goncharov 2002; Abarzhi, Glimm & Lin 2003; Mikaelian 2003; Sohn 2003; Zhang & Guo 2016; Zhang, Deng & Guo 2018; Guo & Zhang 2020; Zhao *et al.* 2020; Zhang & Guo 2022; Liu, Zhang & Xiao 2023). Then, it was extended by Hecht *et al.* (1994) to investigate vacuum bubbles in RMI. Mikaelian (1998) and Zhang (1998) were among the first to give the entire evolutions of bubble and spike, respectively, in a fluid-vacuum configuration. Goncharov (2002) generalized LPM to an arbitrary density ratio, but failed to describe a spike (Mikaelian 2008). Recently, Zhang & Guo (2016), Guo & Zhang (2020) and Zhang & Guo (2022) developed a universal theory for the evolution of fingers (both bubble and spike) with arbitrary density ratio, which was further employed to solve the RTI problem in cylindrical geometry (Zhao *et al.* 2020). More recently, Liu *et al.* (2023) introduced a dual-source (DS) model within the LPM framework to accurately predict interfacial fingers at all density ratios in two and three dimensions.

Under the original LPM framework, the sinusoidal potential function is employed to describe the flow immediately around the fingertip with the constraint of approximately constant surface pressure. This strategy proves a success in describing the growth rate compared with the results from numerical simulations. However, most of these theories assume that the shape of the fingertip does not change with time in the prediction of the growth rate, which conflicts with numerical simulations from Sohn (2004) and Ramaprabhu & Dimonte (2005). According to Liu *et al.* (2023), such an unphysical assumption accounts for the distinct inaccuracy in attempts to catch the concavity and convexity of the fingertip-growth curve as well as the so-called 'overshoot' phenomenon (shown in figure 1). Therefore, shape evolution can be crucial to describe the entire

evolution of interfacial perturbations accurately. To this end, Liu *et al.* (2023) introduced a DS potential function and coupled the solution of growth rate with that of shape curvature.

The DS model (Liu *et al.* 2023) accurately predicts growth rate and shape evolution, and reveals the nonlinear coupling interaction between them. It is also found that such nonlinear interaction leads to a time delay for the emergence of extreme values in the growth rate and shape curvature. Despite the encouraging achievements, one may raise the following questions about the physical mechanism behind the DS results, which motivates the present study. First of all, in the framework of LPM, can one find a universal mathematical expression of the coupling between the growth rate and shape evolution with arbitrary forms of velocity potential functions? Additionally, is there a decomposition method to precisely quantify the effects of potential force and interface evolution, as well as their interaction? Moreover, how do the initial parameters of the interface, e.g. the initial amplitude and shape curvature, alter the interface evolution and, as a result, influence the fingertip growth?

In this paper, it is found that the interfacial growth rate is dominated by two decoupled effects and the underlying physical mechanisms are highlighted based on the LPM framework. We quantify the inertial effect, which is induced by the density difference between fluid species, and the frontal distortion effect, which stems from interface shape evolution. High-fidelity numerical simulation data from Sohn (2004) and Dimonte & Ramaprabhu (2010) are used to verify our model. The sensitivity of interface evolution to initial parameters is also discussed in depth. The remaining paper is structured as follows. The theoretical basis and derivations of the decoupled mechanism are given in § 2. The theoretical analysis and discussions of the decoupled effects are given in § 3. The proposed mechanism is validated for both RTI and RMI flow regimes in § 4. The explanation of potential physical phenomenon through the decoupled mechanism is given in § 5. Conclusions and discussions are made in § 6.

2. Decoupled mechanisms of interface growth rate

For convenience of the subsequent discussion, it is necessary to give an introduction to the LPM. Specifically, we consider a 2-D system of incompressible, inviscid and irrotational flow subject to gravitational acceleration g. In this system, two fluids with different densities are separated upstream and downstream by an interface in a vertically infinite strip with left and right boundaries satisfying the no-penetration condition. The initial material interface is characterized by a single-mode sinusoidal perturbation. The governing equations for the above system can be written as follows per Liu *et al.* (2023):

$$\nabla^2\varphi_i = 0; \tag{2.1}$$

$$\dot{\eta} - \varphi_{i,x}\eta_x + \varphi_{i,z} = 0,\ z = \eta; \tag{2.2}$$

$$\sum_{i=1}^{2} (-1)^i \rho_i \left[-g\eta + \dot{\varphi}_i - \tfrac{1}{2}(\varphi_{i,x}^2 + \varphi_{i,z}^2)\right] = f(t),\ z = \eta. \tag{2.3}$$

Here x and z are the coordinates perpendicular and parallel to the acceleration g, the subscripts $i = 1, 2$ denote the upstream and downstream fluids, respectively, φ_i is the velocity potential function and $f(t)$ depends only on time t. According to the LPM, the interface is approximated as a parabola of the form $\eta(x, t) = z_0(t) + \xi(t)x^2$. Here, $z_0(t)$ and $\xi(t)$ are the vertical position and curvature of the fingertip, which capture the growth rate and shape evolution, respectively. In the present configuration, the curvature is always

non-positive, i.e. $\xi(t) \leq 0$. It needs to be mentioned that the traditional LPM only describes the flow in the neighbourhood of the fingertip instead of the whole region. Therefore, (2.2) and (2.3) are solved on $z = \eta(x, t)$, which avoids invalidity of the potential function hypothesis far away from the fingertip due to the vorticity generated in the flow field. The above 2-D LPM for RTI can be easily extended to the 3-D case with cylindrical symmetry (Goncharov 2002; Guo & Zhang 2020). To that end, the z axis represents the density gradient (axial) direction and the x axis is interpreted as the radial direction by assuming a cylindrical symmetry of the fingers.

Based on the LPM, the evolution of interface growth can be solved from (2.1)–(2.3) provided that a specific expression of φ_i is given. Therefore, the key is to construct a proper velocity potential function φ_i in the LPM. In previous studies most researchers continue to use the classical LPM potential function, which models the system with only primary modes (k, $2k$) and obtains a good approximation for finger growth rate (see, e.g. Mikaelian 1998; Zhang 1998; Goncharov 2002; Abarzhi *et al.* 2003; Mikaelian 2003; Sohn 2003). There are also some scholars who mimic the collective behaviour of all modes exceeding the primary mode k in potential function to obtain a universal curve of finger growth rate (see, e.g. Zhang & Guo 2016; Guo & Zhang 2020). In addition, some other scholars introduce source(s) in the potential function to improve the predictability of finger curvature (see, e.g. Kull 1983, 1986; Zufiria 1988; Sohn & Zhang 2001). Recently, Liu *et al.* (2023) proposed a DS potential function to predict the growth rate and shape evolution simultaneously. Formally, all previous potential functions are subject to the same boundary conditions consistent with the general solution (part or all terms) of the Laplace equation. For a plane RTI system, the general solution of a velocity potential function that satisfies the Laplace equation (2.1) with the corresponding boundary conditions can be given in a series form,

$$\varphi_i(x, z, t) = \sum_{n=1}^{\infty} a_i^n(t) \cos[(2n-1)kx] \exp((-1)^i(2n-1)kz), \tag{2.4}$$

$$\varphi_i(x, z, t) = \sum_{n=1}^{\infty} a_i^n(t) \mathrm{J}_0[(2n-1)kx] \exp((-1)^i(2n-1)kz). \tag{2.5}$$

Here (2.4) and (2.5) are the solutions for 2-D and 3-D cases, respectively; $k \equiv 2\pi/\lambda$ is the wavenumber, J_0 is the Bessel function of zeroth order and $a_i^n(t)$ are unknown variables that depend only on time t. Meanwhile, a signed Atwood number $A \equiv (\rho_1 - \rho_2)/(\rho_1 + \rho_2) \in [-1, 1]$ is introduced to realize a unified description for bubbles and spikes (Zhang & Guo 2016). According to such a definition, one considers bubbles by setting $A > 0, g > 0$ to describe light fluid penetrating into heavy fluid with a downward acceleration, and spikes by setting $A < 0, g < 0$ to describe heavy fluid penetrating into light fluid with an upward acceleration. We comment that $a_i^n(t)$, $z_0(t)$ and $\xi(t)$ also depend on physical parameters A, g and k. For conciseness, we do not display them explicitly. It should be mentioned that only odd terms of n are retained in (2.4) and (2.5) to avoid the imaginary component in the solution (Goncharov 2002).

In this paper the aim is to explore the underlying physical mechanisms of nonlinear coupling between growth rate and shape curvature (Liu *et al.* 2023). Therefore, the general forms of potential functions (2.4) and (2.5) are considered without exploration of the influence of the specific potential function form on the accuracy of the model. In addition, the 2-D case is taken as an example in the following theoretical analysis since there is no essential difference between 2-D and 3-D cases in theoretical solutions.

First, substituting the 2-D general solution φ_i (2.4) into (2.2), one can obtain

$$(v+\dot{\xi}x^2)-2\xi x\left(\sum_{n=1}^{\infty}a_i^n(2n-1)k\sin[(2n-1)kx]\exp((-1)^i(2n-1)kz_0)\right)$$
$$-((-1)^i\sum_{n=1}^{\infty}a_i^n(2n-1)k\cos[(2n-1)kx]\exp((-1)^i(2n-1)kz_0))=0. \tag{2.6}$$

Here, $v\equiv \mathrm{d}z_0/\mathrm{d}t$ is defined as the growth rate of the fingertip. By expanding the trigonometric function and power series shown in (2.6) to order x^{2n-1} (n is the number of unknowns), the unknown variables a_i^n can be solved explicitly and expressed as a function of variables v, ξ and $\dot{\xi}$. Then, substituting the resultant expressions for φ_i into (2.3), one arrives at

$$\sum_{i=1}^{2}(-1)^i\rho_i\left\{g(z_0+\xi x^2)+\left(\sum_{n=1}^{\infty}\dot{a}_i^n(t)\cos[(2n-1)kx]\exp((-1)^i(2n-1)kz)\right)\right.$$
$$+\frac{1}{2}\left[\left(\sum_{n=1}^{\infty}a_i^n(2n-1)k\sin[(2n-1)kx]\exp((-1)^i(2n-1)kz_0)\right)^2\right.$$
$$\left.\left.+\left(\sum_{n=1}^{\infty}a_i^n(2n-1)k\cos[(2n-1)kx]\exp((-1)^i(2n-1)kz_0)\right)^2\right]\right\}=f(t). \tag{2.7}$$

After expanding the trigonometric function and power series in (2.7), one can obtain an ordinary differential equation for the term x^2,

$$\dot{v}+F_1\ddot{\xi}+F_2v^2+F_3v\dot{\xi}+F_4\dot{\xi}^2+F_5g=0. \tag{2.8}$$

Here, $F_{i=1,\ldots,5}(A,k,\xi)$ are functions of the Atwood number A, wavenumber k and curvature ξ, and their concrete expressions depend on the specific form of φ_i. Zhang & Guo (2016) suggest that the curvature ξ is insensitive to time and can be treated as a constant, which leads to $\dot{\xi}=0$ and $\ddot{\xi}=0$. Thus, a simplified ordinary differential equation can be obtained in the form

$$\dot{v}+F_2v^2+F_5g=0. \tag{2.9}$$

In this case, the interface growth rate v depends only on Atwood number A and acceleration g in the whole evolution process. Note that the growth rate given by (2.9) is closely associated with inertial forces and the density difference between two fluids. The velocity thereby obtained is described as the growth rate induced by inertial effects. This nonlinear differential equation is consistent with previous theories (Zhang & Guo 2016; Guo & Zhang 2020) and the specific expressions of F_i can be written according to the corresponding velocity potential function. However, the assumption of ξ as a time-insensitive constant is in conflict with numerical simulations from Sohn (2004) and Ramaprabhu & Dimonte (2005) and may cause unphysical predictions in growth rate (Krechetnikov 2009). Furthermore, the theoretical result given by Liu *et al.* (2023) insists that the curvature plays a crucial role in the prediction of concavity and the overshoot phenomenon during the velocity evolution, which is consistent with existing numerical simulations. Hence, it is argued that the growth rate and shape curvature could be equally important and both should be involved in the theoretical modelling procedure of classical

hydrodynamic instabilities. In light of the above consideration, attention is fixed again on the analysis of (2.8). As can be seen from (2.8), the evolution of v is nonlinearly coupled with the frontal curvature ξ. Therefore, a new variable V is defined as the linear combination of the growth rate v and the curvature term $F_1\dot{\xi}$ to represent the inertial effect, which takes the form

$$V \equiv v - F_1\dot{\xi}. \tag{2.10}$$

Here, $\dot{\xi}$ is the first derivative of curvature and can be regarded as the interfacial curvature change rate. The term $F_1\dot{\xi}$ in (2.10) denotes the frontal distortion induced by the shape evolution accordingly. Using the newly defined V, (2.8) can be rewritten as

$$\dot{V} + F_2V^2 + F_5g + C_0 = 0, \tag{2.11}$$

where $C_0 = (F_3 + 2F_1F_2)v\dot{\xi} + (F_4 - 2F_1^2F_2)(\dot{\xi})^2$ is the residual term and only determined by the property of the Laplace equation. Some useful conclusions can be drawn by comparing (2.9) with (2.11). If C_0 is a small quantity and can be ignored, the new variable V in (2.11) can be regarded as the velocity induced by the inertial effect, which has been explained in (2.9). Additionally, the inertia term (V) and the curvature term ($F_1\dot{\xi}$) are decoupled from each other if (2.10) is rewritten as $v \equiv V + F_1\dot{\xi}$. Therefore, it is the linear combination of these two effects that determines the growth rate of the interface v. In § 3 the relative importance of C_0 will be verified and the analytic expressions of both effects will also be given for both RTI and RMI regimes.

3. Approximate decomposition of the nonlinear mechanism

In order to demonstrate whether C_0 in (2.11) is negligible and consequently the growth rate can be decomposed into two effects in § 2, a specific velocity potential function φ_i is required to obtain the analytical expression for F_i in (2.8). As discussed in § 2, the classical LPM potential functions do not take into account the nonlinear coupling between growth rate and curvature. This is mainly due to the fact that the classical LPM potential functions apply the expansion term x^2 of the interfacial kinematic equation (2.2) for the heavy fluid to solving the curvature, which leads to an equation of the form $\dot{\xi} = f(\xi, v)$. In other words, the curvature evolution in this process is determined only by the heavy fluid and is not fully constrained by the fluids on both sides. By contrast, the strong nonlinear interaction between the growth rate and shape evolution of fingers is taken into consideration in the DS model proposed by Liu *et al.* (2023). Specifically, the expansion terms x^2 and x^4 of the momentum equation (2.3) are used to solve the curvature coupled with the growth rate, leading to a coupled system of equations $\dot{\xi} = f(\xi, v, A)$ and $\dot{v} = g(\xi, v, A)$. As a result, the theoretical prediction of growth rate and curvature is in good agreement with numerical results (Sohn 2004). Without loss of generality, the first two terms of velocity potential function $\varphi_i(n = 1, 2)$ are extracted from the general solution of the (2.4). Then, the specific velocity potential function is substituted into momentum equation (2.3) to obtain the expansion terms x^2 and x^4, which are employed to consider the constraint of both fluids on the curvature evolution. Finally, the analytical expressions of F_i in (2.8)

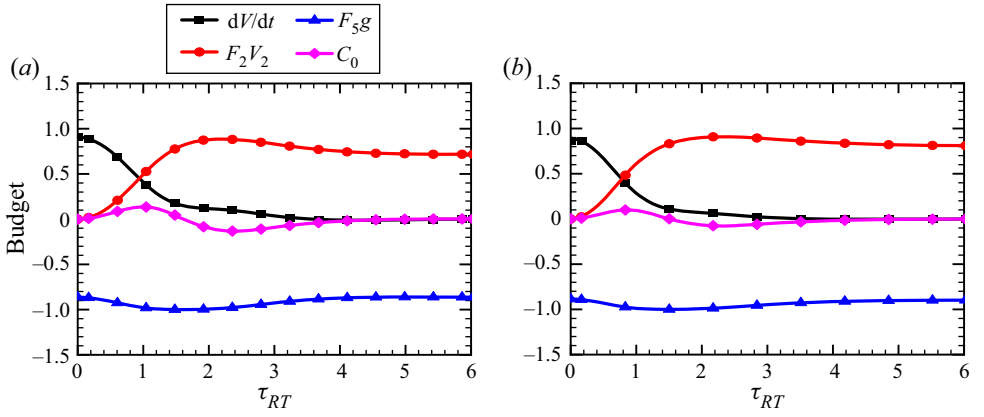

Figure 2. The budget of (2.11) for (*a*) $A = 0.3$ and (*b*) $A = 0.7$. All terms are normalized by the maximum absolute value of gravitational acceleration term $F_5 g$.

take the following forms:

$$\left.\begin{aligned} F_1 &= -[6A\xi - 4k]/[6k^3 + 7Ak^2\xi - 36A\xi^3], \\ F_2 &= [9k^4(4Ak^2 - 12k\xi + 9A\xi^2)]/[2(4k^2 - 9\xi^2)(6k^3 + 7Ak^2\xi - 36A\xi^3)], \\ F_3 &= -[15k^2(4Ak^2 - 12k\xi + 9A\xi^2)]/[(4k^2 - 9\xi^2)(6k^3 + 7Ak^2\xi - 36A\xi^3)], \\ F_4 &= [8(4Ak^2 - 12k\xi + 9a\xi^2)]/[(4k^2 - 9\xi^2)(6k^3 + 7Ak^2\xi - 36A\xi^3)], \\ F_5 &= [4A\xi(4k^2 - 9\xi^2)]/[6k^3 + 7Ak^2\xi - 36A\xi^3]. \end{aligned}\right\} \tag{3.1}$$

Here, $F_i(A, k, \xi)$ are functions of the Atwood number A, wavenumber k and curvature ξ. It can be seen from (3.1) that only the curvature ξ is unknown in a specific case. Note that the curvature evolution can be given based on the DS model (Liu *et al.* 2023), which proves to be approximately consistent with the numerical simulation (Sohn 2004). Thus, combining (3.1) and the solutions for curvature evolutions (Liu *et al.* 2023), one can obtain the evolution solutions for the four terms $\mathrm{d}V/\mathrm{d}t$, F_2V^2, $F_5 g$ and C_0 in (2.11). Shown in figure 2 are temporal evolutions of these four terms for RTI flow. Note that all terms are normalized by the maximum absolute value of the gravitational acceleration term $F_5 g$. For convenience of comparison, a scaled dimensionless time is introduced in the form $\tau_{RT} = \sqrt{Agk}t$, which is the same as that suggested by Goncharov (2002). Two cases with Atwood numbers of 0.3 and 0.7 are selected to show that the present decomposition applies to both high and low Atwood numbers.

As seen in figure 2, the absolute values of F_2V^2 and $F_5 g$ are much larger than that of C_0 except for the very early moment at which both F_2V^2 and C_0 are close to zero. As for $\mathrm{d}V/\mathrm{d}t$, it is much larger than C_0 in the early stage, but gradually approaches C_0 during the evolution, becoming zero together with C_0 in the quasi-steady stage. This is due to the self-similar evolution of RTI with constant velocity in the quasi-steady stage, in which $\mathrm{d}V/\mathrm{d}t$ and C_0 can be neglected when they are compared with F_2V^2 and $F_5 g$. As a result, $\mathrm{d}V/\mathrm{d}t$, F_2V^2 and $F_5 g$ have comparable magnitude, and C_0 can be ignored in the early stage. In the late stage, however, the magnitudes of $\mathrm{d}V/\mathrm{d}t$ and C_0 are much less than those of F_2V^2 and $F_5 g$ such that both can be ignored. Compared with other terms, the value of C_0 is small enough to be ignored in the whole evolution, which confirms that the present consideration of nonlinear coupling between the inertial force and the shape evolution

is reasonable. It is easy to show that the nonlinear term C_0 from (2.11) should not depend on the specific potential function because it is derived from the generalized series form of potential function (2.4). The only possibility for the variation of C_0 may come from the truncation error to the series potential function (2.4). However, it has been manifested that the truncation approximation with the first two terms can account for approximately 95 % of the growth rate Goncharov (2002). It can also be demonstrated that the nonlinear term C_0 remains negligibly small when more terms are retained in the series potential function. For example, the magnitude of C_0 for the present approximation is comparable with that when the series is truncated after the third or fourth term (not shown here for brevity). Thus, (2.11) can be further simplified without substantial loss, which reads

$$\dot{V} + F_2 V^2 + F_5 g = 0. \tag{3.2}$$

Formally, (3.2) is completely consistent with the model equation obtained by Zhang & Guo (2016). The difference is that the fingertip growth rate v_{zg} in the model equation from Zhang & Guo (2016) is determined only by the inertial effect with constant curvature, while V denotes the velocity induced by the inertial effect in (3.2), which is only one part of the fingertip growth rate and allows the variation of curvature. Therefore, one can solve the simplified ordinary differential equation (3.2) to obtain the analytical expression of velocity V induced by the inertial effect in the cases of RMI and RTI, respectively. Furthermore, recalling the definition in (2.10), one can decompose the analytical expressions for fingertip growth rate v into the inertial effect V and the frontal distortion effect $F_1\dot{\xi}$, which are written as

$$v_{RT} = \sqrt{-\frac{F_5}{F_2} g}\,\frac{1-\exp(-2\sqrt{-F_2 F_5 g}t)}{1+\exp(-2\sqrt{-F_2 F_5 g}t)} + F_1\dot{\xi} \quad \text{[RTI]}, \tag{3.3}$$

$$v_{RM} = \frac{V^0}{1+F_2 V^0 t} + F_1\dot{\xi} \quad \text{[RMI]}. \tag{3.4}$$

Here, the superscript 0 indicates initial time. Equations (3.3) and (3.4) give the solutions for the RTI and RMI, respectively. For the RTI, the initial growth rate $v_{RT}^0 = 0$ and the first term is also 0 when $t = 0$. Thus, in order for (3.3) to be satisfied, one ends up with $\dot{\xi}^0 = 0$ by keeping the initial shape of the interface unchanged at the initial moment. For RMI, $g = 0$ in the whole evolution after the impingement of a shock wave. According to (3.2), the inertial effect (V) at the initial time can be obtained from $V^0 = v^0 - F_1\dot{\xi}^0$. Therefore, once the specific velocity potential function is given, the growth rate evolutions for RTI and RMI can be obtained through the above analytical solutions.

It should be pointed out that the results corresponding to the first term in (3.3) and (3.4) have the same form as the theoretical results given by Zhang & Guo (2016) and Guo & Zhang (2020), but with different meanings. Those works assume that the curvature ξ is a time-insensitive constant, which implies that the growth rate is dominated by the inertial acceleration g. The model based on such approximation can successfully predict the evolution trend of the growth rate, but with visible deviations in the nonlinear phase. The present solution suggests that there exists a physical explanation for the deviation between the growth rate and the inertia-induced velocity (the first term in (3.3) and (3.4)). The deviation observed by Zhang & Guo (2016) and Guo & Zhang (2020) is caused by the curvature change rate, which plays a crucial role in the evolution of growth rate at the nonlinear stage and cannot be ignored in the theoretical model.

To summarize, the underlying physical mechanisms of interface evolution in single-mode hydrodynamic instabilities are twofold. One is the inertial effect induced

by the density difference of two fluids, and the other is the frontal distortion effect induced by interface shape evolution. It ought to be stressed that, although there is a nonlinear coupling between growth rate and shape curvature, the physical mechanisms can be simplified into a linear decoupled form based on reasonable approximation without significant loss, as can be seen from the analytical solutions given by (3.3) and (3.4).

4. Verification for the decoupled mechanism of interface evolution

4.1. *Rayleigh–Taylor instability*

The present decoupled mechanism is first validated for the RTI in comparison with the 2-D numerical simulations carried out by Sohn (2004). The theoretical predictions given by Liu *et al.* (2023) are also presented for a comprehensive evaluation. It should be pointed out that the evolution solutions of velocity and curvature given by the DS model are used to realize (3.3). This is due to the lack of curvature evolution for spikes in numerical simulations (Sohn 2004). According to the above reference data, the governing parameters and initial values are set as $g = 1$, $k = 1$, $\xi^0 = -0.25$ and $\dot{\xi}^0 = 0$. For convenience of comparison, a scaled dimensionless time is introduced in the form $\tau_{RT} = \sqrt{Agk}t$, and a scaled dimensionless velocity is also defined as $v_{RT} = v/v_{qs}$, with v_{qs} being the quasi-steady velocity determined by (3.3), which is the same as that suggested by Zhang & Guo (2016).

Shown in figure 3(*a*,*c*,*e*) are evolutions of the bubble growth rate, and figure 3(*b*,*d*,*f*) are the corresponding spike growth rate for the RTI at $A = 0.05$, $A = 0.3$ and $A = 0.7$, respectively. To shed light on the mechanism of each effect and the coupling between them, the inertial effect (V), frontal distortion effect ($F_1\dot{\xi}$) and the combined growth rate v_{RT} are calculated and plotted together in figure 3.

It can be seen from figure 3 that only considering the inertial velocity can roughly predict the evolution trends of both bubble and spike. Consequently, despite the different behaviours among fingers with various Atwood numbers, all fingers gradually approach the same universal curve and can be approximately described by a single equation in terms of the appropriately scaled dimensionless variables given by (3.3), which is entirely consistent with the results given by Zhang & Guo (2016) and Guo & Zhang (2020). However, as discussed in § 3 (see also Liu *et al.* 2023), there exists a significant nonlinear coupling between the curvature and growth rate in the nonlinear stage, which has a crucial impact in the early stage and even changes the concavity and convexity of the growth rate. For example, the overshoot phenomenon in the nonlinear stage makes the change of interface growth rate no longer monotonic as predicted by the inertial effect, which shows the necessity to introduce the effect of curvature in the theoretical model for accurate prediction of the growth rate before the quasi-steady stage.

Figure 3 also shows that although the magnitude of the frontal distortion effect is much smaller than that of the inertial effect, it strongly affects the growth rate in the nonlinear stage. It is observed that the sign change from negative to positive in the frontal distortion effect corresponds to the alternation from suppression to promotion of velocity development. On the growth rate curve, this is reflected as concave first and then convex, which clearly reveals the modulation effect of the interfacial geometry change on the global drag-buoyancy balance. This result is in consistence with the statement given by Liu *et al.* (2023). Here, we comment that the frontal distortion effect always transitions from suppression to promotion of the growth rate in the nonlinear stage. In the case of a small initial perturbation amplitude, the frontal distortion effect only causes a slight overshoot phenomenon. In the case of a large-magnitude initial disturbance, the frontal distortion

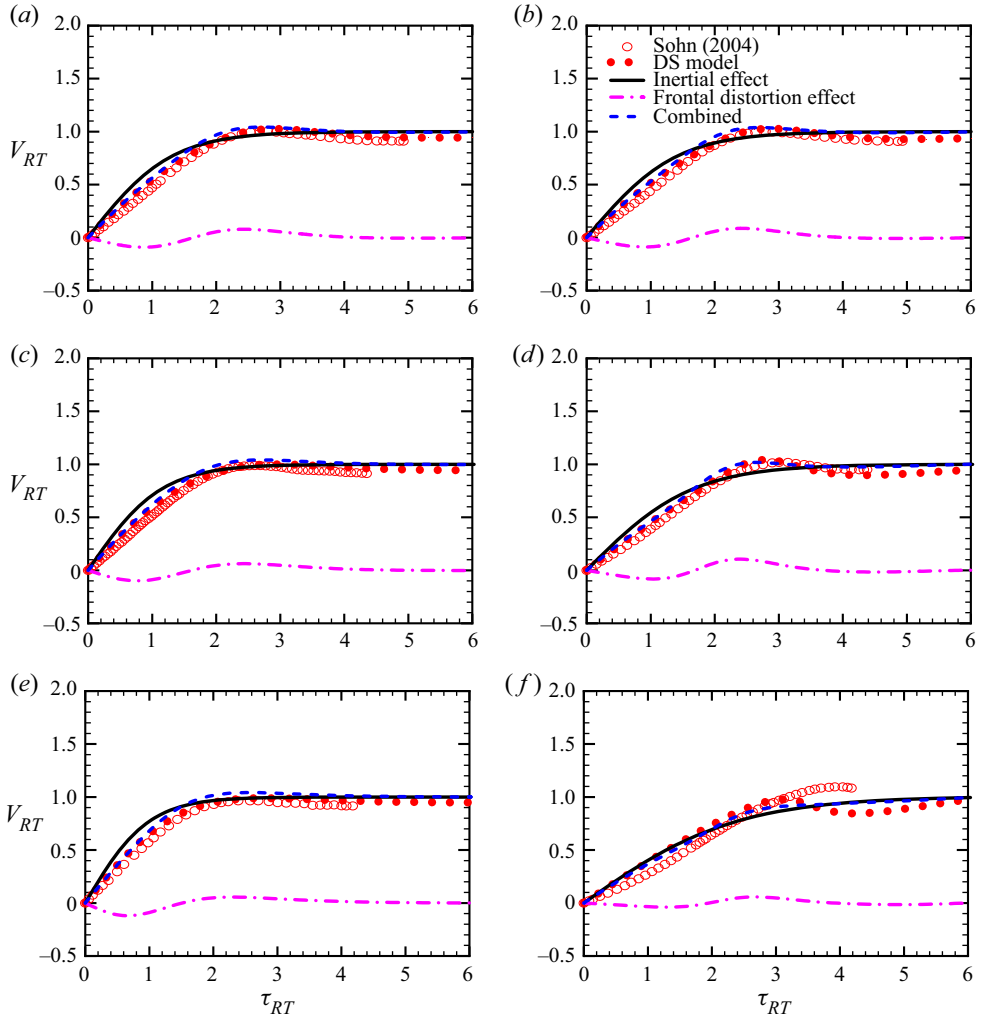

Figure 3. Evolutions of the RTI bubble growth rate (a,c,e) and spike growth rate (b,d,f) at $A = 0.05$, 0.3 and 0.7, which are described by the inertial effect (black solid lines), frontal distortion effect (pink dash-dotted lines) and the total growth rate with combined effects (blue dashed lines), respectively. The results from the DS model (Liu *et al.* 2023) (red dotted lines) and numerical simulation (Sohn 2004) (red circles) are included for comparison. Results are shown for (a) $A = 0.05$ (bubble), (b) $A = -0.05$ (spike), (c) $A = 0.3$ (bubble), (d) $A = -0.3$ (spike), (e) $A = 0.7$ (bubble), (f) $A = -0.7$ (spike).

effect may grow to the same order of magnitude as the growth rate and ultimately change the evolution trend. To demonstrate this point, the initial curvature is altered to adjust the corresponding disturbance in § 5.

On the whole, the theoretical results through inclusion of both the inertial effect and frontal distortion effect are in good agreement with those from numerical simulation (Sohn 2004) and the DS model (Liu *et al.* 2023). This further strengthens the rationality of linear decomposition of the growth rate model (3.3). Although neglect of the nonlinear interaction term C_0 produces slight deviations, the overall results indicate that the retained terms are the dominant factors in the evolution of RTI growth rate. It should be mentioned that the results from the DS model are consistent with those from the numerical simulation

(Sohn 2004) for bubbles at all Atwood numbers and for spikes at $A = 0.05$ and $A = 0.3$. However, a visible difference exists for a spike at $A = 0.7$, as shown in figure 3(f). As argued by Liu *et al.* (2023), this deviation is caused by the strong vorticity at the spike side with the increase of the density ratio of the two fluids. As is clearly seen in figure 3(f), the frontal distortion effect is much weaker than those shown in other panels, which indicates that there exists appreciable error in the prediction of curvature using the DS model for spikes under the condition of high-density ratio. Therefore, the framework of LPM can be questionable on the spike side at high-(negative) Atwood numbers, which may also account for the deviation of the current theory from numerical simulation.

The two proposed mechanisms for RTI evolution indicate that the growth rate induced by acceleration is also affected by the geometric effect of shape evolution. Based on the above analyses, the mechanisms controlling the single-mode interface evolution of RTI can be described as follows. The inertial effect is induced by the density difference of two fluids, which represents the dominant features of growth rate and controls the general trend of flow. The frontal distortion effect is caused by the interface shape evolution and influences the convexity of the fingertip growth curve. According to Mikaelian (2008), the evolution of curvature is determined by the initial condition, and there exists a relation $\xi^0 = -k^2 z_0^0/2$ between the initial curvature and the initial perturbation amplitude. In other words, it is suggested that the nonlinear stage of RTI evolution has a strong dependence on the initial perturbation.

4.2. *Richtmyer–Meshkov instability*

In this section it will be shown that the proposed decoupled mechanism applies not only to the evolution of the RTI but also to that of the RMI, as given by (3.4). After the impingement of a shock wave, the RMI is argued to be approximately equivalent to an incompressible RTI without an external force (Richtmyer 1960; Hecht *et al.* 1994). Again, the decoupled mechanism is validated for the evolution of the RMI in comparison with numerical simulations by Sohn (2004) and Dimonte & Ramaprabhu (2010). The theoretical predictions given by the DS model (Liu *et al.* 2023) are also presented as a necessary complement. For the present decoupled theory to be applied to the RMI, the input parameters are set as $g = 0$, $k = 1$, $\xi^0 = -0.25$ (Sohn 2004) and $\xi^0 = -0.0625$ (Dimonte & Ramaprabhu 2010). For the purpose of visualization, a scaled dimensionless time is introduced in the form $\tau_{RM} = kv^0 t$, and the growth rate is normalized by the velocity after shock wave (i.e. $v_{RM} = v/v^0$), which is consistent with the suggestion by Zhang & Guo (2016). Other settings are the same as in the RTI case.

Shown in figure 4(a,c,e) are evolutions of the bubble growth rate and figure 4(b,d,e) are the corresponding spike growth rate for RMI at $A = 0.3$, $A = 0.7$ and $A = 0.88$, respectively. Here, the initial growth rate v^0 is taken as the rate of fingertip linear growth after the shock wave, which is consistent with the practice in numerical simulations by Sohn (2004); Dimonte & Ramaprabhu (2010). It should be noted that the present decoupled model can well predict bubbles and low-density spikes with the first two terms of velocity potential function $\varphi_i (n = 1, 3)$, but more modes are required to describe the high-density spikes with satisfactory accuracy. Therefore, the coefficients $F_i(A, k, \xi)$ in (3.4) are obtained by retaining the first four terms of the velocity potential function to achieve the prediction of spikes with $A = 0.7$ and $A = 0.88$, respectively. It should be mentioned that the discrepancy in results between the inertial effect and the universal theory of Zhang & Guo (2016) are due to different definitions. Zhang & Guo (2016) directly consider the inertial effect without curvature correction (i.e. $V^0 = v^0$), while

the present inertial effect comes from (3.4) (i.e. $V^0 = v^0 - F_1\dot{\xi}^0$). The summation of inertial and frontal distortion terms provides good prediction for the RMI fingertip growth compared with the DS model and numerical simulation results. The inertia term performs like an envelope of the growth rate curve, depicting the magnitude and damping trend of growth rate curve in the late stage. In the early stage, however, the frontal distortion effect tends to balance the contribution from inertial effect with a comparable magnitude. Furthermore, the rapid change in frontal distortion effect dominates the mathematical features in early time evolution of fingertip growth, such as slope, inflection point and local peak of the growth rate curve.

The frontal distortion effect term in the RMI starts from a negative value and rapidly approaches zero, which is different from the oscillatory behaviour in the RTI case. During its evolution, the first inflection point and the following local maximum value of this frontal distortion term occur immediately after the impingement of the shock wave (see figure 4). Such a phenomenon is named as the early time peak in the present paper and more clearly reflected for all Atwood numbers when the decoupled mechanisms of the two effects are considered. However, the early time peak phenomenon appears only in spike growth rates for the large Atwood number case of the numerical simulations (Sohn 2004; Dimonte & Ramaprabhu 2010) and DS model (Liu *et al.* 2023). The reason for the discrepancy between the present decoupled model and numerical simulation might be the neglect of residual item C_0, which makes the frontal distortion effect more prominent in the RMI regime. Generally, it is believed that the frontal distortion effect indeed causes the early time peak phenomenon, while the coupling of two effects increases the influence of nonlinear interaction item C_0, which makes the early time peak phenomenon weak for bubbles and low-density spikes, but relatively strong for high-density spikes. Similar results are also reported by Zhang & Guo (2022), who believe that the spike curvature can strongly impact the growth rate and should be sensitive to the density ratio. This argument is consistent with our understanding that the frontal distortion effect is not obvious with a small curvature change for bubbles and low-density spikes, but is more pronounced with a drastic curvature change for high-density spikes. Likewise, the intensity of frontal distortion effect depends on the initial magnitudes of curvature and interfacial perturbation. Thus, the frontal distortion effect plays a crucial role in the early evolution of the RMI, which will be further addressed in § 5.

The temporal variations of growth rate shown in figures 3 and 4 suggest that the proposed decoupled mechanism dominates the evolution of both the RTI and RMI. Meanwhile, the comparison between the inertial and frontal distortion effects explains the overshoot phenomenon in the RTI and the early time peak phenomenon in the RMI. The difference lies in the time at which the inflection points and the following extreme values (denoting strong frontal distortion effects) appear according to the decoupled mechanism. Specifically, the overshoot phenomenon appears in the nonlinear stage of the RTI, while the early time peak phenomenon occurs in the early stage of the RMI after the passage of the shock wave.

5. Initial value sensitivity of the frontal distortion effect

It is noteworthy that although the frontal distortion effect is weak compared with the inertial effect, it produces some crucial changes in concavity and convexity of the growth rate curve, e.g. the overshoot phenomenon in the RTI and the early time peak phenomenon in the RMI. As is clearly seen in (3.3) and (3.4), the frontal distortion effect evolves through the second term $F_1\dot{\xi}$. If the independent parameters (such as the acceleration g in the RTI

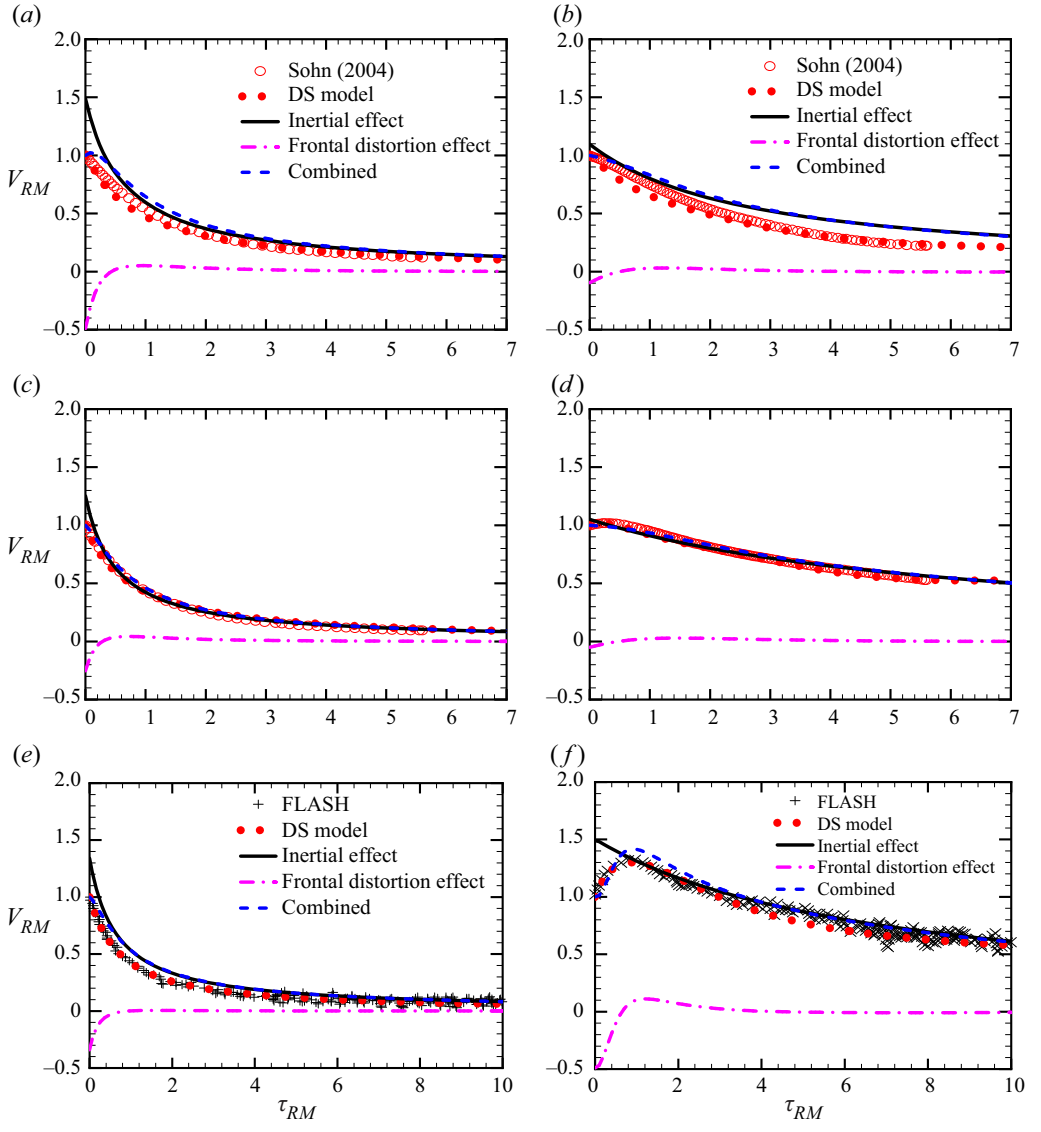

Figure 4. Evolution of the RMI bubble growth rate (*a*,*c*,*e*) and spike growth rate (*b*,*d*,*f*) with $A = 0.3$, 0.7 and 0.88, which are described by inertial effect (black solid lines), frontal distortion effect (pink dash-dotted lines) and the total growth rate with combined effects (blue dashed lines), respectively. The results from the DS model (Liu *et al.* 2023) (red dotted lines), numerical simulation (Sohn 2004) (red circles) and numerical results (FLASH) from Dimonte & Ramaprabhu (2010) ('+' and '×' signs) are included for comparison. Results are shown for (*a*) $A = 0.3$ (bubble), (*b*) $A = -0.3$ (spike), (*c*) $A = 0.7$ (bubble), (*d*) $A = -0.7$ (spike), (*e*) $A = 0.88$ (bubble), (*f*) $A = -0.88$ (spike).

and shock Mach number in the RMI) remain unchanged, and only the material interface is considered, the curvature derivative $\dot{\xi}$ in the early stage will be determined merely by the initial curvature ξ^0. According to Mikaelian (2008), the maximum allowable magnitude of initial curvature ξ^0 is directly restricted by the initial perturbation in the LPM framework, which is also applicable to the present theoretical model. Therefore, reliable results for RTI and RMI evolutions can be obtained with the given initial perturbation as long as the

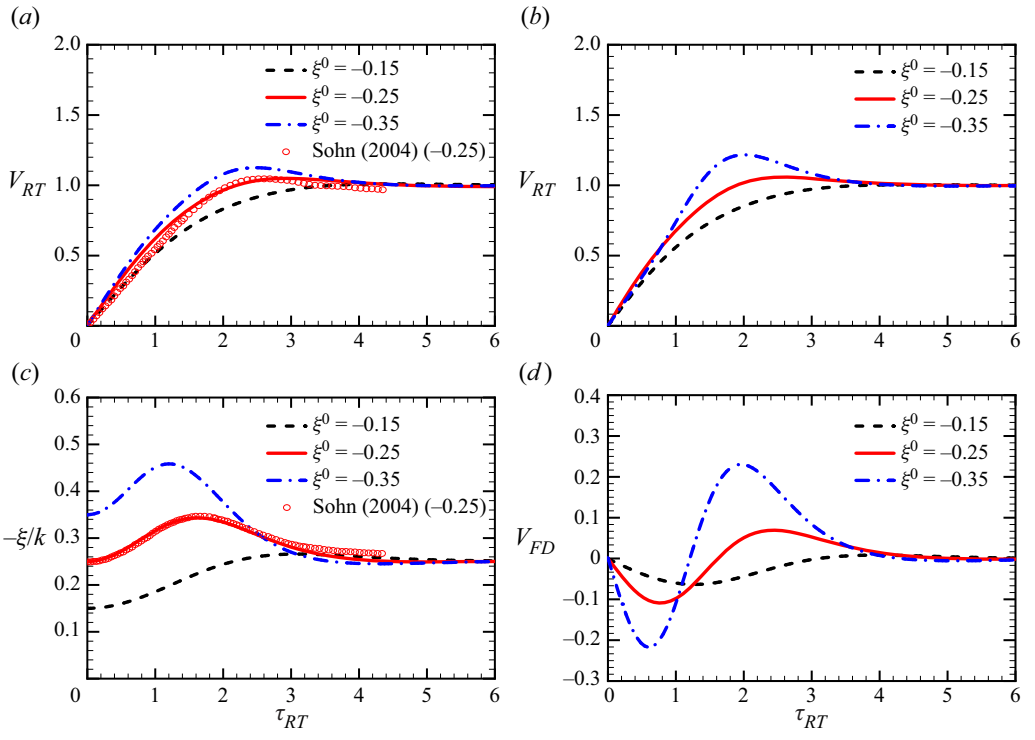

Figure 5. Evolutions of the RTI bubble growth rate predicted by (*a*) the DS model (Liu *et al.* 2023) and (*b*) the decoupled model (3.3) at $A = 0.3$. Evolutions of (*c*) the bubble curvature from the DS model and (*d*) the frontal distortion effect from the decoupled model are plotted for discussion. The results for different initial curvatures are marked as $\xi^0 = -0.15$ (black dashed lines), -0.25 (red solid lines) and -0.35 (blue dash-dotted lines). The numerical simulation results from Sohn (2004) at $\xi^0 = -0.25$ (red circles) are also included for comparison. (*a*) Growth rate (DS model), (*b*) growth rate (decoupled), (*c*) curvature, (*d*) frontal distortion effect.

initial curvature ξ^0 is within the allowable range. Then, the influence of initial curvature on the interface growth rate is investigated by using the decoupled model in comparison with the DS model. As observed in figures 3 and 4 as well as the numerical results from Sohn (2004), the dependence of growth rate on curvature effect almost remains unchanged with Atwood number. Without loss of generality, the case with an Atwood number of 0.3 is taken as an example to discuss the sensitivity of interface growth rate to the initial disturbance. Other settings of the specific parameters, initial values and dimensionless methods are the same as in § 4.

Shown in figure 5(*a*,*c*) are evolutions of the bubble growth rate and the corresponding bubble curvature from the DS model, and figure 5(*b*,*d*) are evolutions of the bubble growth rate given by the decoupled model and the corresponding frontal distortion effect for RTI at $\xi^0 = -0.35$, -0.25 and -0.15, respectively. Here, a scaled dimensionless velocity $v_{FD} = F_1\dot{\xi}/v_{qs}$ is defined based on the frontal distortion effect ($F_1\dot{\xi}$) for convenience of comparison. It should be pointed out that increasing the absolute value of initial curvature from 0.15 to 0.35 corresponds to the increase in amplitude of the initial perturbation. the results given by the DS model compare well with those from numerical simulation (Sohn 2004) for the case of $\xi^0 = -0.25$, which supports the validity of the subsequent discussion. It is further found that, with increasing absolute values of initial curvature, the peak in evolution of the negative curvature becomes higher and is shifted to the left,

which is also consistent with the observations reported by Sohn (2004). The results for growth rate (figure 5*a*,*b*) imply that the overshoot phenomenon is more prominent with the increase of initial perturbation amplitude. This can also be explained by (3.3) and figure 5(*c*,*d*), which indicate that an initial curvature with larger absolute value will cause a more drastic frontal distortion effect due to the larger curvature derivative $\dot{\xi}$ before and after its zero-value time. Here, the discrepancy in growth rate between the DS model and the decoupled model comes from the neglect of the nonlinear interaction term C_0.

According to Mikaelian (2008), the applicability of the LPM is subject to the maximum amplitude of initial perturbations, which varies with the Atwood number A. Here, we try to give a more physical description of this restriction. The absolute ratio of the frontal distortion term to the total growth rate given by the decoupled model is defined as $\chi = |v_{FD}/v_{RT}|$ in order to measure the relative significance of the frontal distortion effect. For the case of $\xi^0 = -0.15$, χ reaches its maximum value of 0.1 at $\tau_{RT} \approx 1.4$. For the case of $\xi^0 = -0.35$, however, the maximum value of χ is approximately 0.75 at $\tau_{RT} \approx 0.6$. The latter shows that the frontal distortion effect may grow to a magnitude comparable to the inertial effect as the initial amplitude increases. In addition, it is seen in figure 5(*d*) that v_{FD} remains negative in almost the whole evolution process for the case of $\xi_0 = -0.15$, which demonstrates that the frontal distortion effect tends to suppress the velocity development in similar cases. By contrast, the suppression stage is followed immediately by a promotion phase for the cases of -0.25 and -0.35, during which the frontal distortion effect has a positive contribution to the velocity development. By comparing figure 5(*b*,*d*), it is seen that the promotion behaviour directly causes the overshoot phenomenon of the growth rate curve. As a result, the lack of frontal distortion effect in LPM will ultimately lead to a deviation in the prediction of growth rate and an underestimation of the overshoot phenomenon.

It is also noted that there exist local maximum or minimum values of RTI bubble velocity and shape curvature during evolution of the interface, which correspond to their critical times. However, the critical times for bubble velocity and shape curvature are different from each other. The mismatch in critical times can be well explained based on (3.3) and the results shown in figure 5(*c*,*d*). Consequently, the growth rate is directly affected by the first derivative of curvature $\dot{\xi}$ rather than the curvature ξ itself, which causes a time delay in the evolution of RTI bubble velocity.

Depicted in figure 6(*a*,*c*) are evolutions of the bubble growth rate and corresponding bubble curvature from the DS model for RMI at $\xi^0 = -0.35$, -0.25 and -0.15. Likewise, figure 6(*b*,*d*) show evolutions of the bubble growth rate given by the decoupled model (3.4) and corresponding frontal distortion effect. Similarly, the validity of the DS model is verified in comparison with the numerical simulation for the case with initial curvature $\xi^0 = -0.25$. The comparisons show that the DS theory can provide reasonable predictions for the RMI growth rate. As for the finger curvature, slight deviations can be observed between the present predictions and numerical simulations by Sohn (2004) in the late stage. Note that the following analysis of initial amplitude influence on RMI development is restricted to the early stage after passage of the shock wave, and therefore, it is still reasonable to discuss the effect of initial curvature based on the DS model.

It is clearly seen from figure 6(*a*,*b*) that, as the absolute value of initial curvature increases, the early time peak phenomenon of the RMI is gradually weakened. Likewise, the weakening of the early time peak in the RMI can be intuitively explained by (3.4); similar to the RTI, the early time peak phenomenon of RMI is mainly caused by the curvature derivative $\dot{\xi}$ before and after its zero-value time. As one can see in figure 6(*c*,*d*), the peak value of the curvature increases when the absolute value of initial curvature

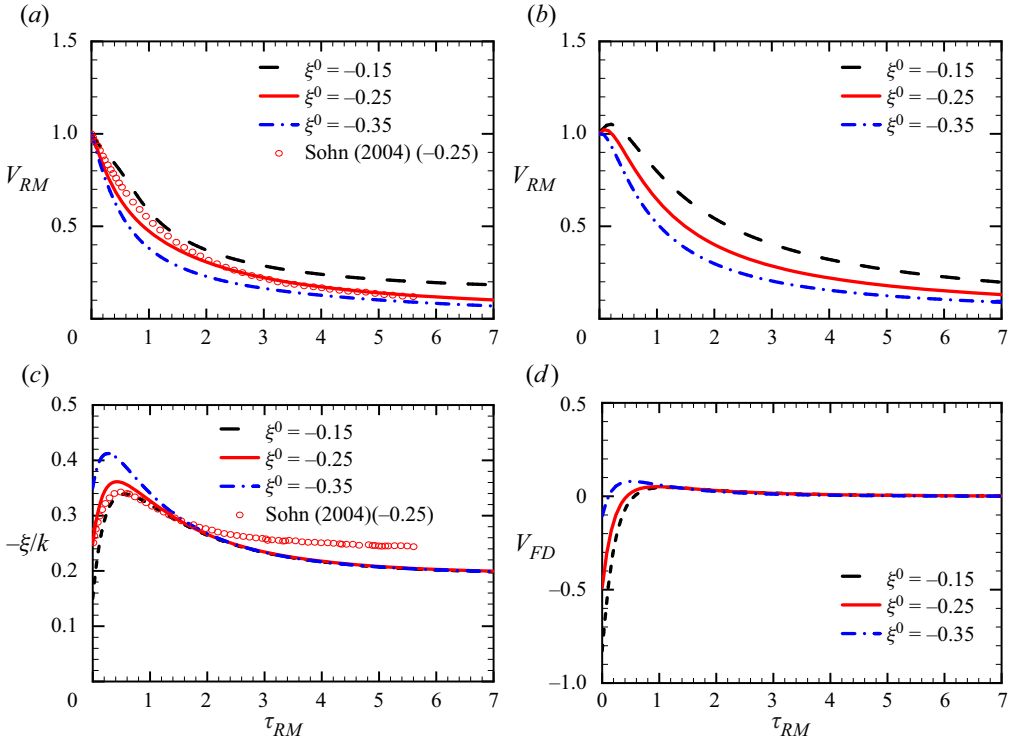

Figure 6. Evolutions of the RMI bubble growth rate predicted by (*a*) the DS model (Liu *et al.* 2023) and (*b*) the decoupled model (3.4) at $A = 0.3$. Evolutions of (*c*) the bubble curvature from the DS model and (*d*) the frontal distortion effect from the decoupled model are plotted for discussion. The results for different initial curvatures are marked as $\xi^0 = -0.15$ (black dashed lines), -0.25 (red solid lines) and -0.35 (blue dash-dotted lines). The numerical simulation results from Sohn (2004) at $\xi^0 = -0.25$ (red circles) are also included for comparison. (*a*) Growth rate (DS model), (*b*) growth rate (decoupled), (*c*) curvature, (*d*) frontal distortion effect.

becomes larger (corresponding to the increase in amplitude of the initial interfacial perturbation), but the initial curvature derivative decreases with the increase of initial curvature. This leads to the weakening of the frontal distortion effect and the early time peak phenomenon when the initial perturbation amplitude becomes larger. In addition, the results in figure 6(*b*,*d*) indicate that the initial curvature can change the concavity of RMI growth rates, which is essentially similar to those observed in figure 5(*b*,*d*) in the RTI. Distinct from the RTI, the combined effect of the decoupled model in the RMI needs more time to gradually approach zero as the initial amplitude increases. It should be pointed out that the discrepancy in growth rate evolution between the DS model and the present decoupled model is more pronounced in RMI, which suggests that the nonlinear coupling between the two effects is stronger in RMI than in RTI and the inclusion of C_0 should suppress the early time peak phenomenon.

Based on the above discussion, we comment that the appearance and intensity of the overshoot and early time peak phenomena strongly depend on the initial curvature, which significantly affects the shape evolution and the interface growth rate. Basically, the essence of these phenomena is the frontal distortion effect, which strongly depends on the initial perturbation amplitude. For a small initial amplitude, the frontal distortion effect is limited to a certain range, which causes the appearance of an overshoot phenomenon in RTI and an early time peak phenomenon in RMI, respectively. For a large initial amplitude,

however, the frontal distortion effect may grow to a magnitude comparable to the inertial effect and ultimately change the growth rate trend, which can lead to the failure of all existing LPMs (Mikaelian 2008). To the authors' knowledge, this is the first theoretical study on the effect of initial curvature, which is important to describe the local geometrical interface of single-mode RTI and RMI.

6. Conclusions and discussions

In this paper the underlying physical mechanism of finger growth rate evolution is explored based on a decoupled model for single-mode interfacial fluid instabilities. The present model takes a linear decoupling form, which is obtained by simplifying the generalized LPM without significant loss and composed of two effects. The inertial effect is induced by the density gradient of two fluids under acceleration, and the frontal distortion effect is induced by interface shape evolution. The analytically decoupled model for these two effects clearly reveal their respective contribution and physical mechanism in comparison with the results given by the DS model (Liu *et al.* 2023) and numerical simulation (Sohn 2004). Specifically, the inertial effect stands for the dominant feature of interface evolution. By contrast, the frontal distortion effect realizes the details of growth rate such as the overshoot phenomenon in the RTI and the early time peak phenomenon in the RMI. The sensitivity of the frontal distortion effect to initial amplitude of perturbation is also addressed to further validate the DS model for prediction of finger growth rate and shape curvature evolution. It turns out that the overshoot phenomenon is enhanced in the RTI, while the early time peak phenomenon is suppressed with the increase of the absolute value of initial curvature, which corresponds to the increase of initial amplitude of perturbation. These phenomena can be well explained through the proposed decoupled mechanism.

It is revealed that the inertial effect represents the movement evolution of the fingertip, and the frontal distortion effect characterizes the geometric changes of the fingertip and its neighbourhood. We comment that they are both important and should be involved in the theoretical modelling of classical hydrodynamic instabilities. For a small initial perturbation amplitude, the frontal distortion effect is relatively weak compared with the inertial effect and has a limited effect on the growth rate, which leads to the occurrence of the overshoot phenomenon and early time peak phenomenon in RTI and RMI, respectively. Nevertheless, the frontal distortion effect may grow to the same order of magnitude as the inertial effect when the initial perturbation amplitude is large enough, and the neglect of curvature evolution may result in an invalid prediction of the instabilities. Therefore, the two effects must be considered simultaneously to predict the fingertip motion more accurately.

Furthermore, the decoupled mechanism proposed in this paper provides the possibility of controlling interfacial instabilities by regulating the initial perturbation amplitude. It is also anticipated that the present decoupled mechanism should be extended to regimes in cylindrical and spherical geometries, for which the geometric effect has yet to be thoroughly studied (Zhou 2017*a*,*b*; Zhao *et al.* 2020). The present study may also pave the way for a further understanding of the re-acceleration stage in single-mode RTI.

Funding. We acknowledge the financial support provided by the National Natural Science Foundation of China (grant nos. 92152202, 11972093, 12222203 and 11988102).

Declaration of interests. The authors report no conflict of interest.

Author ORCIDs.
Yousheng Zhang https://orcid.org/0000-0001-8529-7680;
Zuoli Xiao https://orcid.org/0000-0001-6123-3404.

References

Abarzhi, S.I., Glimm, J. & Lin, A.-D. 2003 Dynamics of two-dimensional Rayleigh–Taylor bubbles for fluids with a finite density contrast. *Phys. Fluids* **15** (8), 2190–2197.

Allred, J.C., Blount, G.H. & Miller, J.H. III 1953 Experimental Studies of Taylor Instability. *Los Alamos Scientific Laboratory Report* LA-1600.

Alon, U., Hecht, J., Ofer, D. & Shvarts, D. 1995 Power laws and similarity of Rayleigh–Taylor and Richtmyer–Meshkov mixing fronts at all density ratios. *Phys. Rev. Lett.* **74**, 534–537.

Betti, R. & Hurricane, O.A. 2016 Inertial-confinement fusion with lasers. *Nat. Phys.* **12** (5), 435–448.

Brouillette, M. 2002 The Richtmyer–Meshkov instability. *Annu. Rev. Fluid Mech.* **34** (1), 445–445.

Burrows, A. 2000 Supernova explosions in the Universe. *Nature* **403** (6771), 727–733.

Casey, D.T., *et al.* 2017 Thermonuclear reactions probed at stellar-core conditions with laser-based inertial-confinement fusion. *Nat. Phys.* **13**, 1227–1231.

Daly, B.J. 1967 Numerical study of two fluid Rayleigh–Taylor instability. *Phys. Fluids* **10** (2), 297–307.

Dimonte, G. & Ramaprabhu, P. 2010 Simulations and model of the nonlinear Richtmyer–Meshkov instability. *Phys. Fluids* **22** (1), 014104.

Ding, J.-C., Ting, S., Yang, J.-M., Lu, X.-Y., Zhai, Z.-G. & Luo, X.-S. 2017 Measurement of a Richtmyer–Meshkov instability at an air-SF_6 interface in a semiannular shock tube. *Phys. Rev. Lett.* **119**, 014501.

Goncharov, V. 2002 Analytical model of nonlinear, single-mode, classical Rayleigh–Taylor instability at arbitrary Atwood numbers. *Phys. Rev. Lett.* **88** (13), 134502.

Guo, W.X. & Zhang, Q. 2020 Universality and scaling laws among fingers at Rayleigh–Taylor and Richtmyer–Meshkov unstable interfaces in different dimensions. *Physica* D **403**, 132304.

Hecht, J., Alon, U. & Shvarts, D. 1994 Potential flow models of Rayleigh–Taylor and Richtmyer–Meshkov bubble fronts. *Phys. Fluids* **6** (12), 4019–4030.

Isobe, H., Miyagoshi, T., Shibata, K. & Yokoyama, T. 2005 Filamentary structure on the Sun from the magnetic Rayleigh–Taylor instability. *Nature* **434**, 478–81.

Jacobs, J.W. & Catton, I. 1988 Three-dimensional Rayleigh–Taylor instability. Part 2. Experiment. *J. Fluid Mech.* **187**, 353–371.

Jacobs, J.W. & Sheeley, J.M. 1996 Experimental study of incompressible Richtmyer–Meshkov instability. *Phys. Fluids* **8** (2), 405–415.

Krechetnikov, R. 2009 Rayleigh–Taylor and Richtmyer–Meshkov instabilities of flat and curved interfaces. *J. Fluid Mech.* **625**, 387–410.

Kull, H.J. 1983 Bubble motion in the nonlinear Rayleigh–Taylor instability. *Phys. Rev. Lett.* **51**, 1434–1437.

Kull, H.J. 1986 Nonlinear free-surface Rayleigh–Taylor instability. *Phys. Rev.* A **33** (3), 1957–1967.

Layzer, D. 1955 On the instability of superposed fluids in a gravitational field. *Astrophys. J.* **122**, 1.

Lewis, D.J. & Taylor, G.I. 1950 The instability of liquid surfaces when accelerated in a direction perpendicular to their planes. II. *Proc. R. Soc. Lond.* A **202** (1068), 81–96.

Lherm, V., Deguen, R., Alboussière, T. & Landeau, M. 2022 Rayleigh–Taylor instability in impact cratering experiments. *J. Fluid Mech.* **937**, A20.

Li, X.-L., Fu, Y.-W., Yu, C.-P. & Li, L. 2021 Statistical characteristics of turbulent mixing in spherical and cylindrical converging Richtmyer–Meshkov instabilities. *J. Fluid Mech.* **928**, A10.

Liang, Y., Zhai, Z.-G., Ding, J.-C. & Luo, X.-S. 2019 Richtmyer–Meshkov instability on a quasi-single-mode interface. *J. Fluid Mech.* **872**, 729–751.

Liu, L.-L., Liang, Y., Ding, J.-C., Liu, N.-A. & Luo, X.-S. 2018 An elaborate experiment on the single-mode Richtmyer–Meshkov instability. *J. Fluid Mech.* **853**, R2.

Liu, C.-W., Zhang, Y.S. & Xiao, Z.-L. 2023 A unified theoretical model for spatiotemporal development of Rayleigh–Taylor and Richtmyer–Meshkov fingers. *J. Fluid Mech.* **954**, A13.

Luo, X.-S., Wang, X.-S. & Si, T. 2013 The Richtmyer–Meshkov instability of a three-dimensional air/SF6 interface with a minimum-surface feature. *J. Fluid Mech.* **722**, R2.

Luo, X.-S., Zhang, F., Ding, J.-C., Si, T., Yang, J.-M., Zhai, Z.-G. & Wen, C.-Y. 2018 Long-term effect of Rayleigh–Taylor stabilization on converging Richtmyer–Meshkov instability. *J. Fluid Mech.* **849**, 231–244.

MATSUO, K., SANO, T., NAGATOMO, H., SOMEKAWA, T., LAW, K.-F., MORITA, H., ARIKAWA, Y. & FUJIOKA, S. 2021 Enhancement of ablative Rayleigh–Taylor instability growth by thermal conduction suppression in a magnetic field. *Phys. Rev. Lett.* **127**, 165001.

MATSUOKA, C., NISHIHARA, K. & FUKUDA, Y. 2003 Erratum: nonlinear evolution of an interface in the Richtmyer–Meshkov instability. *Phys. Rev.* E **68**, 029902.

MESHKOV, E.E. 1969 Instability of the interface of two gases accelerated by a shock wave. *Fluid Dyn.* **4** (5), 101–104.

MIKAELIAN, K.O. 1998 Analytic approach to nonlinear Rayleigh–Taylor and Richtmyer–Meshkov instabilities. *Phys. Rev. Lett.* **80**, 508–511.

MIKAELIAN, K.O. 2003 Explicit expressions for the evolution of single-mode Rayleigh–Taylor and Richtmyer–Meshkov instabilities at arbitrary Atwood numbers. *Phys. Rev.* E **67**, 026319.

MIKAELIAN, K.O. 2008 Limitations and failures of the Layzer model for hydrodynamic instabilities. *Phys. Rev.* E **78**, 015303.

NIEDERHAUS, C.E. & JACOBS, J.W. 2003 Experimental study of the Richtmyer–Meshkov instability of incompressible fluids. *J. Fluid Mech.* **485**, 243–277.

RAMAPRABHU, P. & DIMONTE, G. 2005 Single-mode dynamics of the Rayleigh–Taylor instability at any density ratio. *Phys. Rev.* E **71**, 036314.

RAMAPRABHU, P., DIMONTE, G. & ANDREWS, M.J. 2005 A numerical study of the influence of initial perturbations on the turbulent Rayleigh–Taylor instability. *J. Fluid Mech.* **536**, 285–319.

RAYLEIGH, LORD 1883 Investigation of the character of the equilibrium of an incompressible heavy fluid of variable density. *Proc. Lond. Math. Soc.* **s1-14** (1), 170–177.

RENOULT, M.C., ROSENBLATT, C. & CARLES, P. 2015 Nodal analysis of nonlinear behavior of the instability at a fluid interface. *Phys. Rev. Lett.* **114**, 114503.

RICHTMYER, R.D. 1960 Taylor instability in shock acceleration of compressible fluids. *Commun. Pure Appl. Maths* **13** (2), 297–319.

RISTORCELLI, J.R. & CLARK, T.T. 2004 Rayleigh–Taylor turbulence: self-similar analysis and direct numerical simulations. *J. Fluid Mech.* **507**, 213–253.

SABET, N., HASSANZADEH, H., DE WIT, A. & ABEDI, J. 2021 Scalings of Rayleigh–Taylor instability at large viscosity contrasts in porous media. *Phys. Rev. Lett.* **126**, 094501.

SHARP, D.H. 1984 An overview of Rayleigh–Taylor instability. *Physica* D **12** (1–3), 3–18.

SOHN, S.-I. 2003 Simple potential-flow model of Rayleigh–Taylor and Richtmyer–Meshkov instabilities for all density ratios. *Phys. Rev.* E **67**, 026301.

SOHN, S.-I. 2004 Vortex model and simulations for Rayleigh–Taylor and Richtmyer–Meshkov instabilities. *Phys. Rev.* E **69**, 036703.

SOHN, S.-I. & ZHANG, Q. 2001 Late time behavior of bubbles at unstable interfaces in two dimensions. *Phys. Fluids* **13** (11), 3493–3495.

TAYLOR, G.I. 1950 The instability of liquid surfaces when accelerated in a direction perpendicular to their planes. I. *Proc. R. Soc. Lond.* A **201** (1065), 192–196.

TRYGGVASON, G. & UNVERDI, S.O. 1990 Computations of three-dimensional Rayieigh–Taylor instability. *Phys. Fluids* A **2** (5), 656–659.

WADDELL, J.T., NIEDERHAUS, C.E. & JACOBS, J.W. 2001 Experimental study of Rayleigh–Taylor instability: low Atwood number liquid systems with single-mode initial perturbations. *Phys. Fluids* **13** (5), 1263–1273.

WEI, T. & LIVESCU, D. 2012 Late-time quadratic growth in single-mode Rayleigh–Taylor instability. *Phys. Rev.* E **86**, 046405.

WILKINSON, J.P. & JACOBS, J.W. 2007 Experimental study of the single-mode three-dimensional Rayleigh–Taylor instability. *Phys. Fluids* **19** (12), 124102.

YAN, Z., FU, Y.-W., WANG, L.-F., YU, C.-P. & LI, X.-L. 2022 Effect of chemical reaction on mixing transition and turbulent statistics of cylindrical Richtmyer–Meshkov instability. *J. Fluid Mech.* **941**, A55.

YANG, J., KUBOTA, T. & ZUKOSKI, E.E. 1993 Applications of shock-induced mixing to supersonic combustion. *AIAA J.* **31** (5), 854–862.

ZHANG, Q. 1998 Analytical solutions of Layzer-type approach to unstable interfacial fluid mixing. *Phys. Rev. Lett.* **81**, 3391–3394.

ZHANG, Q., DENG, S.Y. & GUO, W.X. 2018 Quantitative theory for the growth rate and amplitude of the compressible Richtmyer–Meshkov instability at all density ratios. *Phys. Rev. Lett.* **121**, 174502.

ZHANG, Q. & GUO, W.X. 2016 Universality of finger growth in two-dimensional Rayleigh–Taylor and Richtmyer–Meshkov instabilities with all density ratios. *J. Fluid Mech.* **786**, 47–61.

ZHANG, Q. & GUO, W.X. 2022 Quantitative theory for spikes and bubbles in the Richtmyer–Meshkov instability at arbitrary density ratios. *Phys. Rev. Fluids* **7**, 093904.

ZHANG, Q. & SOHN, S.-I. 1996 An analytical nonlinear theory of Richtmyer–Meshkov instability. *Phys. Lett.* A **212** (3), 149–155.

ZHANG, Q. & SOHN, S.-I. 1997 Padé approximation to an interfacial fluid mixing problem. *Appl. Math. Lett.* **10** (5), 121–127.

ZHAO, Z.-Y., WANG, P., LIU, N.-S. & LU, X.-Y. 2020 Analytical model of nonlinear evolution of single-mode Rayleigh–Taylor instability in cylindrical geometry. *J. Fluid Mech.* **900**, A24.

ZHOU, Y. 2017*a* Rayleigh–Taylor and Richtmyer–Meshkov instability induced flow, turbulence, and mixing. I. *Phys. Rep.* **720-722**, 1–136.

ZHOU, Y. 2017*b* Rayleigh–Taylor and Richtmyer–Meshkov instability induced flow, turbulence, and mixing. II. *Phys. Rep.* **723-725**, 1–160.

ZHOU, Y., *et al.* 2021 Rayleigh–Taylor and Richtmyer–Meshkov instabilities: a journey through scales. *Physica* D **423**, 132838.

ZHOU, Y., CABOT, W.H. & THORNBER, B. 2016 Asymptotic behavior of the mixed mass in Rayleigh–Taylor and Richtmyer–Meshkov instability induced flows. *Phys. Plasmas* **23** (5), 052712.

ZHOU, Y., CLARK, T.T., CLARK, D.S., GAIL GLENDINNING, S., AARON SKINNER, M., HUNTINGTON, C.M., HURRICANE, O.A., DIMITS, A.M. & REMINGTON, B.A. 2019 Turbulent mixing and transition criteria of flows induced by hydrodynamic instabilities. *Phys. Plasmas* **26** (8), 080901.

ZUFIRIA, J.A. 1988 Bubble competition in Rayleigh–Taylor instability. *Phys. Fluids* **31** (3), 440–446.